Internal Report IASF-BO 429/2005

October 7, 2005

SIMULATION ASPECTS ON THE ZLE MODELLING IN THE PLANCK MISSION

M. Maris[1], C. Burigana[2], S. Fogliani[1]

[1] *INAF-OAT, via G.B. Tiepolo 11, I-34131, Trieste, Italy*
[2] *INAF-IASF Bologna, via P. Gobetti 101, I-40129, Bologna, Italy*

Internal Report IASF-BO/429/2005

October 7, 2005

SIMULATION ASPECTS ON THE ZLE MODELLING IN THE PLANCK MISSION

M. Maris[1], C. Burigana[2], S. Fogliani[1]

[1] *INAF-OAT, via G.B. Tiepolo 11, I-34131, Trieste, Italy*
[2] *INAF-IASF Bologna, via P. Gobetti 101, I-40129, Bologna, Italy*

SUMMARY – The PLANCK satellite, scheduled for launch in 2007, will produce a set of full sky maps in nine microwave bands spanning from sub-mm to mm, with an unprecedented sensitivity, resolution and sky coverage. Planets, minor bodies and diffuse interplanetary dust will contribute to the (sub)mm sky emission observed by PLANCK representing a source of foreground contamination to be removed before to extract the cosmological information as well as an interesting subject of scientific analysis. In a dedicated paper we presented a new method to simulate the time-dependent level of contamination from ZLE at PLANCK frequencies. In this report we outline some technical details relevant for simulations that have not been included in the paper. We focus on the numerical code, its validation, the detailed series expansion of the ZLE, the definition of colour and emissivity correction, the transforms between the relevant reference systems, and some details on file formats.

1 Introduction

This report is in support of a forthcoming paper (Maris et al. 2005) dedicated to the study of the *Zodiacal Light Emission* (ZLE) in the context of the PLANCK mission. The reader is refereed to that paper for an exhaustive discussion. We focus here on some technical details, omitted for conciseness in the paper, that are relevant in simulations.

The *Zodiacal Light Emission* (ZLE) due to thermal emission from the Interplanetary Dust Particles (IDPs) is the far-infrared (Far-IR) counterpart of the familiar Zodiacal Light due to scattering of the solar light by IDPs. Most of the properties of the ZLE below 300 μm have been studied by IRAS (Wheelock et al. 1994), COBE (Kelsall et al. 1998) and ISO (Reach et al. 1996, Reach et al. 2003). Peaking at $\lambda \approx 10$ μm, the ZLE is one of the major contributors to the sky background in the Far-IR domain at low ecliptic latitudes. A first detection in the 300 μm $-$ 1000 μm band has been assessed by Fixsen & Dwek (2002) using yearly averaged COBE/FIRAS data. Even a quick look to the data reported in Kelsall et al. (1998) and Fixsen & Dwek (2002) allows to predict a contribution of ZLE in the 857 GHz channel of PLANCK of ≈ 0.6 MJy/sr. It is evident that at the PLANCK lowest frequencies its contribution is much weaker than the Galaxy emission. On the other hand, at the PLANCK intermediate and high frequencies the ZLE is significantly weaker than the Galactic emission only at low Galactic latitudes while it is comparable to it outside the Galactic plane (for example, near the poles the Galactic emission is ~ 1 MJy/sr at 857 GHz). The expected ZLE contribution is larger than the instrumental noise at the PLANCK highest frequencies. Therefore, a careful analysis of the ZLE in the PLANCK data is required.

Our starting point to reconstruct the spatial distribution of the ZLE, is the model of Kelsall et al. (1998) for the ZLE based on the COBE data (hereafter indicated as *COBE-model*) has many similarities with the IRAS model by Wheelock et al. (1994). It describes in details the emissivity of the IDPs cloud, assumed to extend up to $\simeq 5.2$ AU far from the Sun, for wavelengths up to about 300 μm. According to the COBE-model four components contribute to the ZLE the dominating *Smooth component*, the *Earth orbit locked ring* of dust (or *Circumsolar ring*), the *Trailing blob*, and three *Bands of dust*.

With respect to other foregrounds usually considered in CMB studies, the ZLE (as the other Solar System objects) is peculiar, depending its flux not only on the pointing direction but also on the instantaneous position of the observer within the Solar System. This underlines the relevance of study the ZLE not only on maps but also on time ordered data streams (TODs). Moreover, the simulation of observations for a satellite mission like PLANCK can not be based on maps since the details of the orbit will have to be considered in addition to the usual scanning law.

2 The model and the numerical code

The flux calculated for a given frequency band is

$$F_{ZLE,f}(\mathbf{P}, \mathbf{R}_\odot, \mathbf{R}_\mathrm{P}) = \sum_c F_{c,f}(\mathbf{P}, \mathbf{R}_\odot, \mathbf{R}_\mathrm{P}) = \sum_c E_{c,f} Z_{c,f}(\mathbf{P}, \mathbf{R}_\odot, \mathbf{R}_\mathrm{P}) \,. \qquad (1)$$

Here $\mathbf{R}_\odot$ denotes the positions of the Sun within the Solar System and the index c denotes the specific component either the dominating *Smooth component*, the *Earth orbit locked ring* of dust, the *Trailing blob*, or one of the three *Bands of dust*. According to the discussion in Maris et al. (2005), in Eq. (1) we separate the calculation of the spatial distribution of the ZLE assumed to be a blackbody from the more uncertain emissivity correction $E_{c,f}$. According to this decomposition we separated the geometrical aspects of the model from the frequency scaling.

	Expected Peak Surface brightnesses [Jy/sterad]						
Freq. [GHz]	Smooth Component	Band 2	Trailing Blob	Locked Ring	Band 1	Band 3	Total
30	2.1×10^{2}	7.3×10^{1}	5.7×10^{1}	3.3×10^{1}	1.2×10^{0}	$1.5\times10^{-}1$	3.6×10^{2}
44	5.1×10^{2}	1.6×10^{2}	1.2×10^{2}	7.1×10^{1}	2.5×10^{0}	$3.2\times10^{-}1$	8.2×10^{2}
70	1.5×10^{3}	4.0×10^{2}	3.1×10^{2}	1.8×10^{2}	6.3×10^{0}	$8.1\times10^{-}1$	2.3×10^{3}
100	3.4×10^{3}	8.1×10^{2}	6.3×10^{2}	3.7×10^{2}	1.3×10^{1}	1.7×10^{0}	5.0×10^{3}
143	7.6×10^{3}	1.6×10^{3}	1.3×10^{3}	7.5×10^{2}	2.6×10^{1}	3.4×10^{0}	1.1×10^{4}
217	2.0×10^{4}	3.8×10^{3}	2.9×10^{3}	1.7×10^{3}	5.9×10^{1}	7.7×10^{0}	2.7×10^{4}
353	5.9×10^{4}	9.8×10^{3}	7.6×10^{3}	4.5×10^{3}	1.5×10^{2}	2.0×10^{1}	7.9×10^{4}
545	1.6×10^{5}	2.3×10^{4}	1.8×10^{4}	1.0×10^{4}	3.6×10^{2}	4.6×10^{1}	2.0×10^{5}
857	4.3×10^{5}	5.4×10^{4}	4.3×10^{4}	2.5×10^{4}	8.5×10^{2}	1.1×10^{2}	5.4×10^{5}

	Power Law Parameters						
	Smooth Component	Band 2	Trailing Blob	Locked Ring	Band 1	Band 3	Total
β	0.278	-0.027	-0.019	-0.026	-0.037	-0.029	0.183
$\frac{J_{\mathrm{peak}}}{1\mathrm{Jy/sterad}}$	4.45×10^{5}	5.57×10^{4}	4.39×10^{4}	2.53×10^{4}	8.65×10^{2}	1.13×10^{2}	5.42×10^{5}

Table 1: Expected peak surface brightnesses for the ZLE components at different Planck frequencies (upper frame) and coefficients for the power law fit (lower frame).

2.1 The spatial distribution in the COBE model

Fig. 1 represents the relevant geometry of ZLE observations assuming either the ecliptic barycentric of heliocentric reference system. Relevant elements are the Sun, (eventually the barycentre of the Solar System $B_{\rm SS}$), the position of the L_2 point, the PLANCK position $\mathbf{R}_{\rm P}$, the centre of the distribution of dust related to the component c of interest, C_c, and the related vectors drawn between these points. The most important among them are: the position of a point at distance s from the spacecraft along the pointing direction $\mathbf{P}$: $\mathbf{R}(s) = \mathbf{R}_{\rm P} + s\mathbf{P}$; its position with respect to the Sun $\mathbf{R}_{\rm s} = \mathbf{R} - \mathbf{R}_{\odot}$ and to the centre of the cloud defined by $\mathbf{R}_{0,c}$: $\mathbf{R}'_c = \mathbf{R} - \mathbf{R}_{0,c}$. In addition we define $R'_c = |\mathbf{R}'_c|$. X'_c, Y'_c, Z'_c denote the Cartesian components of $\mathbf{R}'_c$ and X, Y, Z those of $\mathbf{R}$. For each component c it is possible to define a proper reference frame about which the cloud c has cylindrical symmetry. Its origin coincides with the centre of the considered component; its midplane may be rotated, tilted and shifted with respect to the ecliptic plane. The transformation rules between the relevant reference frames are reported in App. 6.

The model assumes that the 3D density distribution of each component is factorised into a radial component, describing the density distribution as a function of the distance from the cloud centre, and a vertical component, describing the density distribution as a function of the height over the cloud midplane:

$$Z_c = X'_c \sin\Omega_c \sin i_c - Y'_c \cos\Omega_c \sin i_c + Z'_c \cos i_c, \tag{2}$$

where i_c and Ω_c are respectively the inclination and ascending node of the midplane as seen from the Sun.

According to Eq. (1) of Maris et al. (2005), the spatial distribution of flux $Z_{f,c}(\mathbf{P}, \mathbf{R}_{\odot}, \mathbf{R}_{\rm P})$ is

$$Z_{f,c}(\mathbf{P}, \mathbf{R}_{\odot}, \mathbf{R}_{\rm P}) = \int_0^{+\infty} n_c(\mathbf{r}(s)) B_f(T(\mathbf{r}(s))) K_f(\nu)\, ds\,, \tag{3}$$

where $n_c(\mathbf{r})$ is the local 3D-density for the component c, $B_f(T)$ is the blackbody brightness at the central frequency of the frequency band, K_f is an instrument dependent colour-correction factor, $T(s)$ is the temperature of an IDP grain at distance s from the spacecraft, and at distance $R_{\rm s}(s)$ from the Sun, given the pointing direction $\mathbf{P}$. The model assumes:

$$T(R_{\rm s}) = \frac{T_0}{R_{\rm s}^{\delta}}\,. \tag{4}$$

The most probable value of δ ($= 0.467$) is very close to the theoretical value of 0.5 for large grey grains in radiative equilibrium (Kelsall et al. 1998), while $T_0 = 286$ K.

The spatial density of the *Smooth component* is then

$$n_{SMOOTH}(\mathbf{R}'_c) = n_{0,SMOOTH} \left|\mathbf{R}'_c\right|^{-\alpha} f(\zeta), \tag{5}$$

$$\zeta = \left|\frac{Z_c}{R_c}\right|, \tag{6}$$

$$f(\zeta) = \exp(-\beta g^{\gamma}), \tag{7}$$

$$g = \begin{cases} \zeta^2/2\mu & \text{for } \zeta < \mu \\ \zeta - \mu/2 & \text{for } \zeta \geq \mu \end{cases}. \tag{8}$$

where β (not to be confused with the geocentric ecliptic latitude), γ, and μ are free parameters of the model.

For a *Band of dust* we have

$$n_{Bi}(\mathbf{R}'_c) = \frac{3n_{3Bi}}{R}\left[v_{Bi}+\left(\frac{\zeta_{Bi}}{\delta_{\zeta_{Bi}}}\right)^{p_{Bi}}\right]\left\{1-\exp\left[-\left(\frac{R}{\delta_{R_{Bi}}}\right)^{20}\right]\right\}\exp\left[-\left(\frac{\zeta_{Bi}}{\delta_{\zeta_{Bi}}}\right)^{6}\right] \quad (9)$$

$$\zeta_{Bi} = \left|\frac{z_{Bi}}{R_c}\right| \quad (10)$$

where n_{3Bi} is the density at 3 AU of band i ($i = 1, 2, 3$) and $\delta_{\zeta_{Bi}}, v_{Bi}, p_{Bi}\ \delta_{R_{Bi}}$ are adjustable shape parameters.

For the *Earth orbit locked ring* of dust we have

$$n_R(\mathbf{R}'_c) = n_{0,SR}\exp\left[-\frac{(R-R_{SR})^2}{2\sigma^2_{rSR}}\right]\exp\left[-\frac{|Z_R|}{\sigma_{zSR}}\right], \quad (11)$$

where the σ values are free parameters for the scale lengths in R and Z_R. R_{SR} is the radial location of the peak density of the ring.

For the *Trailing blob* we have

$$n_{TB}(\mathbf{R}'_c) = n_{0,TB}\exp\left[-\frac{(R-R_{TB})^2}{2\sigma^2_{rTB}}\right]\exp\left[-\frac{|Z_R|}{\sigma_{zTB}}\right]\exp\left[-\frac{(\theta-\theta_{TB})^2}{2\sigma^2_{\theta TB}}\right], \quad (12)$$

where the σ values are free parameters for the scale lengths in R, Z_{TB}, and θ coordinates. R_{TB} is the radial locations of the peak density of the blob. The θ coordinate is the difference between the ecliptical longitude of the spacecraft and that of the Sun. The list of parameters for each component from Kelsall et al. (1998) is reported in Tab. 2 for the sake of completeness.

2.2 The simulation code

We have implemented the model described in the previous sections in a `FORTRAN-90/95` program called `FS_ZOD` (FLIGHT SIMULATOR ZODIACAL LIGHT EMISSION) [1] that computes $Z_f(\mathbf{P}, \mathbf{R}_\odot, \mathbf{R}_P)$ for a given list of values of $\mathbf{P}$, $\mathbf{R}_\odot$, $\mathbf{R}_P$ and a set of parameters describing the properties of the ZLE component for which the calculation has to be performed.

Since the E_f scalings are largely uncertain, the code separately generates the fluxes appropriate to each desired component. The outputs produced for the various components can be then easily combined according to the user need.

The data streams from `FS_ZOD` may be added to other simulated signals or used as they are to generate TODs and then maps, angular power spectra, etc. . In Maris et al. (2005) we used the code to study the time dependence in the signal acquired by PLANCK for the nominal scanning strategy (Dupac & Tauber 2005) and to predict the ZLE signal.

We choose to express our results in terms of brightness (MJy/sr), as for IRAS and COBE/DIRBE data.

The `FS_ZOD` is part of a pipeline written in `OCTAVE` [2]. The pipeline reads the list of pointing and positions, drives `FS_ZOD` to perform the calculation, collects the results, organises them in tables, `FITS` files and secondary products, performs the series expansion described in

[1] Although the code was originally designed as a module of the PLANCK Flight Simulator in the current implementation it can be applied to any other experiment.

[2] www.octave.org.

Sect. 3, generates postprocessing graphics, and monitors the execution generating reports and statistics.

The code has been implemented to run on a single processor or on a Beowulf system multiprocessor machine. The system used for this work is a 6 processors Beowulf system, each unit having an `Intel` CPU with 700 MHz of Clock, 1 MByte cache, 5 GBytes of RAM and operated under Red Hat 9.0 OS with GNU compilers. Further informations and details on code verification, validation, and performances are in Maris (2001). The single CPU time needed to perform a calculation for a combination of $\mathbf{P}$, $\mathbf{R}_P$, $\mathbf{R}_\odot$ and f and for a single receiver is $(1 \pm 0.2) \times 10^{-3}$ sec including the I/O overhead.

The `FS_ZOD` is validated comparing the output with an `OCTAVE` implementation of the ZLE model which may be operated by the pipeline. The `OCTAVE` version is validated against the results in Kelsall et al. (1998) and a simplified ZLE model for which an analytical form exists. Validation tests are standardized and distributed with the pipeline, so at each new release of `FS_ZOD` the validation may be repeated automatically.

component	parameter	definition	value	1σ uncertainty
Smooth Cloud	$n_{0,smooth}$	density at 1 AU	1.13×10^{-7} AU $^{-1}$	6.4×10^{-10}
	α	radial power law exponent	1.34	0.022
	β	vertical shape parameter	4.14	0.067
	γ	vertical power law exponent	0.942	0.025
	μ	widening parameter	0.189	0.014
	i	inclination	2.03°	0.017
	Ω	asc. node	77.7°	0.6
	X_0	x offset from Sun	.0119 AU	0.0011
	Y_0	y offset from Sun	.00548 AU	0.00077
	Z_0	z offset from Sun	$-.00215$ AU	0.00043
Dust Band 1	$n_{3,B1}$	density at 3 AU	5.59×10^{-10} AU^{-1}	7.20×10^{-11}
	$\delta_{\zeta_{B1}}$	shape parameter	8.78°	-
	υ_{B1}	shape parameter	.10	-
	p_{B1}	shape parameter	4	-
	i_{B1}	inclination	0.56°	-
	Ω_{B1}	asc. node	80°	-
	$\delta_{R_{B1}}$	inner radial cutoff	1.5 AU	-
Dust Band 2	$n_{3,B2}$	density at 3 AU	1.99×10^{-9} AU^{-1}	1.28×10^{-10}
	$\delta_{\zeta_{B2}}$	shape parameter	1.99°	-
	υ_{B2}	shape parameter	.90	-
	p_{B2}	shape parameter	4	-
	i_{B2}	inclination	1.2°	-
	Ω_{B2}	asc. node	30.3°	-
	$\delta_{R_{B2}}$	inner radial cutoff	.94 AU	0.025
Dust Band 3	$n_{3,B3}$	density at 3 AU	1.44×10^{-10} AU^{-1}	2.34×10^{-11}
	$\delta_{\zeta_{B3}}$	shape parameter	15.0°	-
	υ_{B3}	shape parameter	.05	-
	p_{B3}	shape parameter	4	-
	i_{B3}	inclination	0.8°	-
	Ω_{B3}	asc. node	80.0°	-
	$\delta_{R_{B3}}$	inner radial cutoff	1.5 AU	-
Solar Ring	$n_{0,SR}$	density at 1 AU	1.83×10^{-8} AU^{-1}	1.27×10^{-9}
	R_{SR}	radius of peak density	1.03 AU	0.00016
	σ_{rSR}	radial dispersion	0.025 AU	-
	σ_{zSR}	vertical dispersion	0.054 AU	0.0066
	i_{RB}	inclination	0.49°	0.063
	Ω_{RB}	asc. node	22.3°	0.0014
Trailing Blob	$n_{0,TB}$	density at 1 AU	1.9×10^{-8} AU^{-1}	1.42×10^{-9}
	R_{TB}	radius of peak density	1.06 AU	0.011
	σ_{rTB}	radial dispersion	0.10 AU	0.0097
	σ_{zTB}	vertical dispersion	0.091 AU	0.013
	θ_{TB}	longitude w.r.t. earth	-10°	-
	$\sigma_{\theta TB}$	longitude dispersion	12.1°	3.4

Table 2. Table of parameters for the ZLE model, for all the components the integration is carried on up to an outer radius of $R_{cutoff} = 5.1$ AU, adapted from Kelsall et al. (1998).

3 Series Expansion of the ZLE Spatial Dependence

Simulators for CMB missions and the related data-reduction pipelines as those realized for PLANCK, are largely based on maps. A map allows a good representation of the sky brightness as a function of the pointing direction. This procedure neglects the time dependent information on the PLANCK position within the Solar System, leading to a loss of information when Solar System components are considered. The ground segment of a mission like PLANCK would be in fact able to handle and analyse TODs as well as maps obtained from them (Pasian & Sygnet 2002, van Leeuwen et al. 2002, Challinor et al. 2002). A TOD of ZLE would allow an exact representation of any seasonal dependence. However, TODs are large and their realization is strictly related to the effective scanning strategy and satellite orbit, possibly accommodated during the mission, so that the exchange of simulated data in the form of TODs is not a practical perspective for the data analysis of a multichannel, high-resolution mission like PLANCK. We implemented a method able to: 1. properly represent seasonal effects in a large set of mission configurations; 2. be possibly applied to other missions; 3. exploit the (cylindrical) symmetries in the components of the IDPs cloud.

We propose to generalise the usual concept of *pixelized map*. A pixelized map is usually defined as the values assumed by a given observable on a set of pixels ordered according to the adopted pixelization scheme. In this contest we can introduce a generalisation of this concept by defining a pixelized "map" as a list of values assumed by a given observable on a set of pixels which are also functions of the positions of the Sun ($\mathbf{R}_\odot$) and of the Spacecraft (PLANCK in our case) ($\mathbf{R}_\mathrm{P}$) within the Solar System. It is easy to recognise that in a reference frame (r.f.) in which the displacements of the Sun and spacecraft positions are just small fractions of their averaged positions, the pixelized "map" can be replaced by the series expansion of the observable about the average positions of the Sun and the Spacecraft.

Since we are interested here to the Smooth component, we adopt as r.f. for the series expansion evaluation a r.f. X, Y, Z centred on the center of the Smooth cloud, having as fundamental plane (X, Y) the symmetry plane of the cloud, but rotated around the axis normal to the symmetry plane to have the spacecraft on the plane $Y = 0$. We name this r.f. the *Corotanting symmetry reference frame*. Sect. 6 reports the equations to transform pointing directions, spacecraft and Sun positions between this r.f. and the ecliptic r.f..

Then denoting with $\overline{\mathbf{R}}_\mathrm{P}$, $\overline{\mathbf{R}}_\odot$ the reference positions of PLANCK and Sun about which the series expansion is performed, we have

$$\mathbf{R}_\mathrm{P} = \overline{\mathbf{R}}_\mathrm{P} + \delta\mathbf{R}_\mathrm{P}, \quad \mathbf{R}_\odot = \overline{\mathbf{R}}_\odot + \delta\mathbf{R}_\odot. \tag{13}$$

In the numerical computations we exploit values of the displacements along each direction up to about ± 0.03 AU for $\delta\mathbf{R}_\odot$ and up to about ± 0.07 AU for $\delta\mathbf{R}_\mathrm{P}$, about a factor of two wider than any reasonable displacement for a mission which will reside near L_2. In addition, we adopt in this work the `HEALPix` scheme (Górsky et al. 2005), widely used within the CMB community. Since PLANCK will scan the sky in nearly great circles drawn about a spin axis kept at an angle less then 10° from Sun - Spacecraft direction, for computational purposes it is preferable to work with a Cartesian *"map" r.f.* defined as the corotanting symmetry r.f. but with the $\hat{Z}$ axis oriented along the line connecting the Smooth cloud Center to the reference spacecraft position $\overline{\mathbf{R}}_\mathrm{P}$ away from the center, while $\hat{X}$ is drawn on the symmetry plane and $\hat{Y}$ orthogonal to it, within this reference frame then

$$\overline{\mathbf{R}}_\mathrm{P} = [0.0, 0.0, 1.01] \quad \mathrm{AU}, \quad \overline{\mathbf{R}}_\odot = [0.0, 0.0, 0.0] \quad \mathrm{AU}. \tag{14}$$

Moreover, since PLANCK will scan only a 8° wide band about the telescope axe, we compute the series expansions only for the band of directions effectively observed by PLANCK, in order

to reduce the computational effort, albeit the method can be straightforwardly applied to other experiments. The *ring* ordering of the `HEALPix` scheme is particularly advantageous to identify the pixels of the above band.

We have tested that in the case of the ZLE it is preferable to expand in power series not the brightness spatial distribution but its logarithm. Then, denoting with $Z_{f,c,p}(\mathbf{R}_\odot, \mathbf{R}_\mathrm{P})$ the brightness integral for a given frequency channel f, component c and pixel index p (connected to the pointing direction $\mathbf{P}$ by the mapping scheme) as a function of $\mathbf{R}_\odot$ and $\mathbf{R}_\mathrm{P}$ we adopt the following decomposition

$$Z_{f,c,p}(\mathbf{R}_\odot, \mathbf{R}_\mathrm{P}) = \overline{Z}_{f,c,p} F_{\mathrm{S},f,c,p}(\delta\mathbf{R}_\odot) F_{\mathrm{P},f,c,p}(\delta\mathbf{R}_\mathrm{P}) F_{\mathrm{PS},f,c,p}(\delta\mathbf{R}_\odot, \delta\mathbf{R}_\mathrm{P}), \tag{15}$$

where $\overline{Z}_{f,c,p} \equiv Z_{f,c,p}(\overline{\mathbf{R}}_\odot, \overline{\mathbf{R}}_\mathrm{P})$ and $F_{\mathrm{S},f,c,\mathbf{P}}(\delta\mathbf{R}_\odot)$, $F_{\mathrm{P},f,c,\mathbf{P}}(\delta\mathbf{R}_\mathrm{P})$, $F_{\mathrm{PS},f,c,\mathbf{P}}(\delta\mathbf{R}_\odot, \delta\mathbf{R}_\mathrm{P})$ are exponential functions of polynomials of $\delta\mathbf{R}_\odot$ and $\delta\mathbf{R}_\mathrm{P}$. We verified that, in order to reach an accuracy better than $\simeq 1\%$ for more than 96% of the pixels [3], it is enough to consider the following terms of the series expansion:

$$\log F_{\mathrm{S},p}(\delta\mathbf{R}_\odot) = a_{\mathrm{S},p,i}\delta R_{\odot,i} + b_{\mathrm{S},p,ij}\delta R_{\odot,i}\delta R_{\odot,j}; \tag{16}$$

$$\log F_{\mathrm{P},p}(\delta\mathbf{R}_\mathrm{P}) = a_{\mathrm{P},p,i}\delta R_{\mathrm{P},i} + b_{\mathrm{P},p,ij}\delta R_{\mathrm{P},i}\delta R_{\mathrm{P},j} + c_{\mathrm{P},p,ijk}\delta R_{\mathrm{P},i}\delta R_{\mathrm{P},j}\delta R_{\mathrm{P},k}; \tag{17}$$

$$\log F_{\mathrm{SP},p}(\delta\mathbf{R}_\odot\delta\mathbf{R}_\mathrm{P}) = b_{\mathrm{SP},p,ij}\delta R_{\odot,i}\delta R_{\mathrm{P},j}, \tag{18}$$

where $\delta R_{\odot,i}$ and $\delta R_{\mathrm{P},i}$, $i = X, Y, Z$, are the Cartesian components of $\delta\mathbf{R}_\odot$ and $\delta\mathbf{R}_\mathrm{P}$; a, b, and c terms denote the first, second, and third order coefficients, respectively, and repeated indices i, j, $k = X$, Y, Z are summed. This is a good compromise between the accuracy needed in these kinds of applications and the economy of the data set. To avoid to over-complicate the notation, from here we will not explicit the dependence on p, f and c, except where explicitely written. The number of independent coefficients is 3 for $a_{\mathrm{S},p,i}$ and $a_{\mathrm{P},p,i}$, 6 for $b_{\mathrm{S},p,ij}$ and $b_{\mathrm{S},p,ij}$, 9 for $c_{\mathrm{P},p,ijk}$ and $b_{\mathrm{SP},p,ij}$. The other coefficients are simply obtained by index permutations. Then, for each pointing direction a total number of (1) + (3 + 6) + (3 + 6 + 9) + 9 = 38 independent components has to be computed. These coefficients can be determined by solving a sufficiently high set of independent equations obtained by exploiting different combinations of displacements $\delta\mathbf{R}_\mathrm{P}$, $\delta\mathbf{R}_\odot$. After some tests, we verified that a good stability of the solution can be achieved by calculating for about 100 combinations of $\delta\mathbf{R}_\mathrm{P}$, $\delta\mathbf{R}_\odot$ the fluxes for each pixel in the map and determining the coefficients by least squares. For each pixel, the code evaluates also the residuals of the fit to $Z_{f,c,p}$ defined as

$$\Delta Z_{f,c,p}(\delta\mathbf{R}_\odot, \delta\mathbf{R}_\mathrm{P}) = Z^{\mathrm{fit}}_{f,c,p}(\delta\mathbf{R}_\odot, \delta\mathbf{R}_\mathrm{P}) - Z^{\mathrm{numerical}}_{f,c,p}(\delta\mathbf{R}_\odot, \delta\mathbf{R}_\mathrm{P}) \tag{19}$$

allowing the generation of various metrics representing the quality of the approximation. Among them, the most important are the maximum absolute and relative residuals

$$\mathcal{E}_p = \max_{(\delta\mathbf{R}_\odot, \delta\mathbf{R}_\mathrm{P})} (|\Delta Z_{f,c,p}(\delta\mathbf{R}_\odot, \delta\mathbf{R}_\mathrm{P})|) \tag{20}$$

$$\mathcal{E}_{\mathrm{r},p} = \max_{(\delta\mathbf{R}_\odot, \delta\mathbf{R}_\mathrm{P})} \left(\frac{|\Delta Z_{f,c,p}(\delta\mathbf{R}_\odot, \delta\mathbf{R}_\mathrm{P})|}{Z^{\mathrm{numerical}}_{f,c,p}(\delta\mathbf{R}_\odot, \delta\mathbf{R}_\mathrm{P})} \right) \tag{21}$$

calculated over the values obtained by exploiting all the considered displacements for each pixel, proving the accuracy of this expansion discussed above.

[3] The remaining pixels will have an accuracy worst then 1% (the worst accuracy recorded being 2.5%) in the case of a displacement of the spacecraft and of the Sun at the limits of the region for which the expansion is calculated.

Finally, the computed coefficients are stored in `HEALPix - FITS` files organised as binary tables according to the following conventions

1. a row for each pixel ordered according to the ring scheme (columns of not used pixels are filled with `NaN`);
2. pixel index p is the row number of the table, pixels are ordered according to the *ring* scheme;
3. each row is composed of columns grouped as it follows

$$\mathrm{row}_p := \left(\overline{Z}, \mathbb{F}_\mathrm{S}, \mathbb{F}_\mathrm{P}, \mathbb{F}_\mathrm{SP}, \mathcal{E}, \mathcal{E}_\mathrm{r}\right)_p \tag{22}$$

   (a) the first column is $\overline{Z}_{f,c,p}$ usually expressed in MJy/sr,

   (b) the last two columns are the errors defined in eqs. (20) and (21) expressed in units consistent to $\overline{Z}$,

   (c) intermediate $\mathbb{F}_s$ (with s the *sector index* s = S, P, SP) blocks represents the coefficients for the F_s functions. Each block is hierarchically structured as:

$$\mathbb{F}_s := (\mathbb{A}_s, \mathbb{B}_s, \mathbb{C}_s, \dots) \tag{23}$$

   with $\mathbb{A}_s = a_{s,i}, i = X, Y, Z$ the set of first order coefficients for sector s, $\mathbb{B}_s = b_{s,ij}$ the set of independent second order coefficients for sector s, and so on. Note that for the sector SP the only group of coefficients is of the b kind.

4. In the `FITS` header the proper self consistent mapping of each column and the relevant information to use the file is reported.

A dedicated `IDL` library to simply handle these files named `ZLE_IDL` has been created (Maris et al. 2004).

The time needed to complete a ZLE "map" of expansion series for $N_\mathrm{side} = 256$ is 32 hours for a single CPU. The execution time is scales nearly linearly with ${N_\mathrm{side}}^2/N_\mathrm{cpu}$, N_cpu being the number of CPUs or Beowulf units.

4 K_f and E_f definition

We explicitly derive from Eq. (1) of Maris et al. (2005) the approximation in Eq. (2) in the same paper. With the notation of Sect. 2 of Maris et al. (2005) we approximate Eq. (1) of the same paper with the product $F_f E_f K_f$ [4], where F_f is the integral in Eq. (2) of Maris et al. (2005) computed along the LOS, E_f, and K_f are the effective emissivity and the colour correction to be determined for the given frequency band. From here we will omit the pointing dependence to simplify the notation. Then

$$F_f E_f K_f \approx \frac{1}{\Delta f} \int_\mathrm{BW} W_f(\nu) \epsilon(\nu) \mathcal{F}_f(\nu) d\nu \; ; \tag{24}$$

taking in account that both $\mathcal{F}_f(\nu)$ and $\epsilon(\nu)$ scales as power laws in our limited bandwidth and Taylor expanding in the log - log space about $\log f$ the brightness, $\log \mathcal{F}_f(\nu) = \log \mathcal{F}_f(f) + \mathcal{F}'_f(f)(\log \nu - \log f) + \mathcal{O}(2)$, and the emissivity correction, $\log \epsilon(\nu) = \log \epsilon(f) + \epsilon'(f)(\log \nu -$

[4] We assume a relative bandwidth $\beta_f < 1$ (for PLANCK $\beta_f = 0.2 - 0.25$, and we assume f the central frequency of the bandwidth $\mathrm{BW} \equiv f(1 - \beta_f/2) \leq \nu \leq f(1 + \beta_f/2)$ we want to approximate the complete brightness integral for a given LOS Eq. (1) of Maris et al. (2005) with the product $I_{0,f} E_f K_f$.

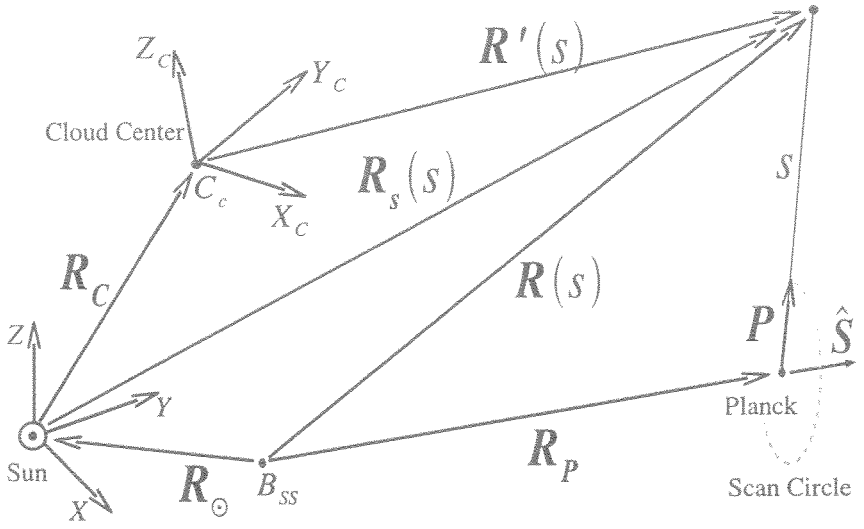

Figure 1: Relations between the heliocentric and cloud-centred frames used to describe the Solar System scanning geometry for a mission like PLANCK. The relations between Planck, Sun, Cloud Center and the observed portion of cloud are drawn, the L_2 point is not drawn to simplify the graph. The connection between the other two reference frames is shown in Fig. 7. An example of scan circle and the related spin axis, $\hat{\mathbf{S}}$, are also drawn. The graph is not in scale with real distances.

$\log f) + \mathcal{O}(2)$, with $\mathcal{F}'(f)$ and $\epsilon'(f)$ short hands for $d\log\mathcal{F}_f/d\log\nu|_{\nu=f}$, $\frac{d\log\epsilon}{d\log\nu}|_{\nu=f}$, from Eq. (24) we obtain

$$F_f = \mathcal{F}_f(f), \quad E_f = \epsilon(f), \quad K_f = \frac{1}{\Delta f}\int_{\mathrm{BW}} W_f(\nu)\left(\frac{\nu}{f}\right)^{\epsilon'(f)+\mathcal{F}'_f(f)} d\nu\ ; \tag{25}$$

assessing the correctness of the aforementioned expansion.

Note that in Kelsall et al. (1998) the colour correction is defined as a correction for the instrumental response when a blackbody is observed.

For this reason the colour correction is parametrised as a function of the blackbody temperature T which is a function of the position along the line of sight, so that the argument of the pointing direction integral in Eq. (2) of Maris et al. (2005) would have to be scaled by the spatial dependent $K_f(T)$.

However, at our frequencies the bulk of the blackbody emissivity comes from grains emitting not too far from the Rayleigh-Jeans limit, i.e. with a power law scaling as a function of the frequency within our rather limited bandwidth, with the power law index largely independent from T. In this conditions the two definitions for K_f are equivalent.

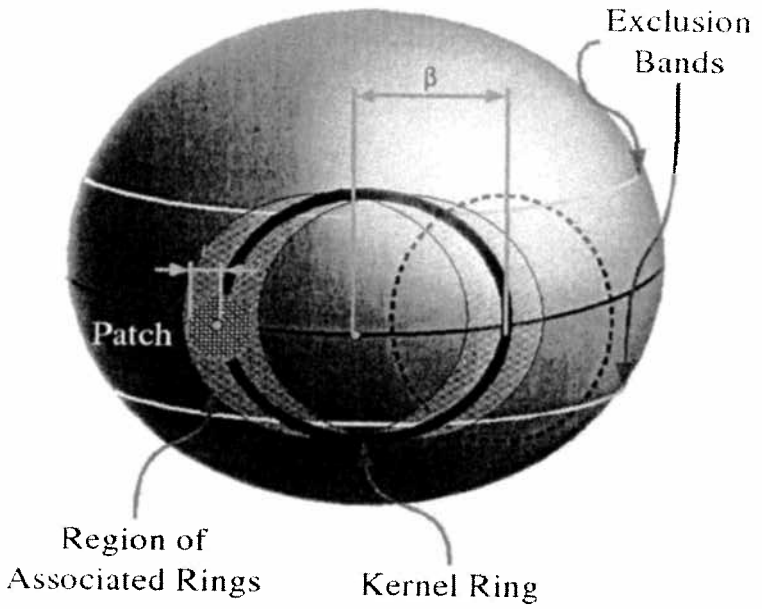

Figure 2: Patching scheme for scan circles drawn along the equator, of radius β and patches of radius r. The figure shows the kernel circle of choice (red-thick), another kernel circle (black, dashed) and the region of scan circles associated to the kernel (grey, dashed area). A circular patch at the crossing between the equator (black, full line) and the kernel is also displayed (circle with red border and blue hatching), as the upper and lower limit of the exclusion bands (grey, full lines).

5 Scanning Strategy and Setup of Sky Patches

In Maris et al. (2005) circular patches in the sky at the crossing of two PLANCK scans of the sky are composed, but the algorithm to construct such patches and the list of patches is not reported. In particular requirements for the construction of patches are:

1. each patch shall be made of samples of sky observerd in the first and in the second survey, samples unobserved in one of the two surveys shall be discarded;
2. each patch shall be composed of an identical number of samples belogin to each survey;
3. noise in scan circles shall be statistically independent (avoid sharing of samples between patches);
4. samples of each survey within a given patch shall be selected assessing maximal differences in satellite positions during their observation.

The last requiremet is the hardest to accomodate since scan circles has the tendency to pile-up near the ecliptical poles (Dupac & Tauber 2005). Many and many days of observation may contribute to the same patch near the pole smearing out the differential effects we want to measure with PLANCK.

Patches are build-up on the definition of scan circles within a survey.

5.1 Definition of the Patching Scheme

A scan circle is defined by

1. its angular radius β;

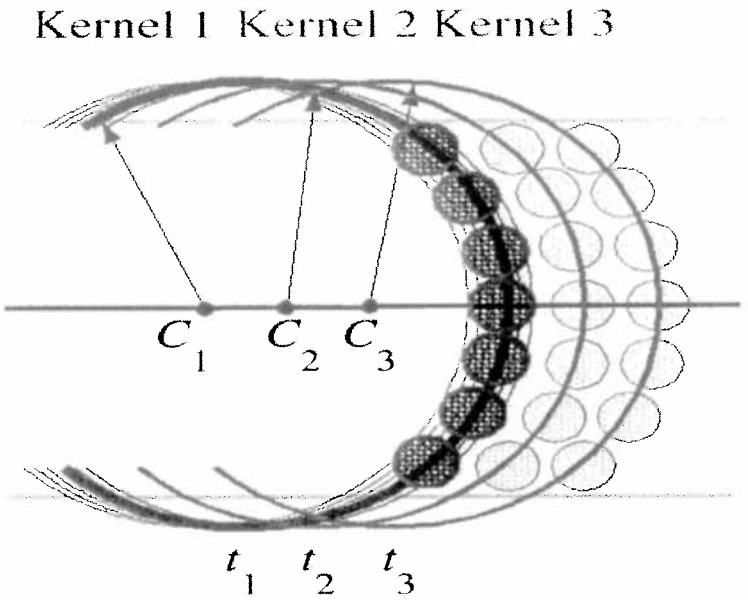

Figure 3: Example of patching for three consecutive kernel scan circles. Colors follows Fig. 2. Thin black lines are the scan circles associated to Kernel 1 with times defined by Eq. (26). All the kernels have patches at the crossing with the equator, while the other patches are simmetrically distributed about it up to the begin of the exclusion bands.

2. the axis passing through its center $\check{\mathbf{C}}$ in the sky;
3. the epoch of acquisition t.

The scanning strategy defines

1. the value of β assumed for all the circles;
2. the list of consecutive epochs t at which each circle has been acquired;
3. the list of centers $\check{\mathbf{C}}_t$ for each epoch;
4. the list of positions of the satellite within the Solar System for each epoch.

Patches are defined by

1. the patch radius r;
2. the patch center;
3. the epoch intervall in which the samples in the patch have been acquired.

In addition, in the remaining part of this discussion we assumed that

1. during the acquisition of a scan circle (for PLANCK 1 hour) the satellite does not change appreciably its position within the Solar System;
2. PLANCK scans the sky according to the *Nominal* scanning strategy [5] (Dupac & Tauber 2005), where it is assumed that PLANCK is stepping the sky acquiring scan circles

   with centers on the ecliptical equator;

[5] The procedure may be generalized for other scanning strategies.

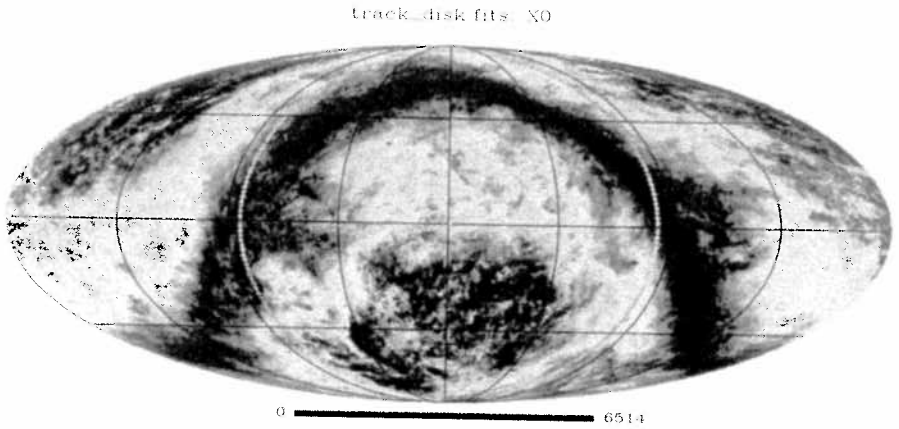

Figure 4: Grey spots are circular patches of 2° radius, drawn along a scan circle acquired within a single survey. Spots are overlapped to a map of Galaxy at 857GHz.

at constant time intervals Δt,

at constant discrete angular intervalls $\Delta\theta$,

with zero dead times between the end of a scan circle and the begin of the next one.

Fig. 2 and Fig. 3 details the explanation of the following two-steps patching algorithm, for patches of fixed width r. Examples of patching of a sky map in `HEALPix` are shown in Fig. 4 and Fig. 5.

Step A The list of time-ordered scan circles in each survey is partitioned according to the following procedure

1. select a set *kernel scan circles* in the survey

   kernel scan circles shall have they centers at distances greater than $2r$,

   kernel scan circles shall be time-ordered and consecutive in time;

2. for each kernel scan circle define the set of *associated scan circles* in the survey

   associated scan circles shall be neighbour in time to their kernel scan circle,

   centers of associated scan circles shall depart from the center of the kernel no more than $\pm r$.

Step B Patches are drawn

1. in the regions defined by the scan circles belonging to each partition class;
2. to avoid pile-up effects patches are not drawn over regions where scan circles belonging to different classess overposes or cross (definining exclusion regions toward the poles);
3. patches are drawn at distances equal or greater than $2r$ along the kernel scan circle;
4. patches are distributed symmetrically about the equator within the limits imposed by the exclusion bands, the first patch is located at the crossing point between the equator and the kernel.

In particular for the stepping scanning strategy of PLANCK the scan circles entering each class of angular width $2r$ are those acquired at times

$$t_k - \Delta t \frac{r}{\Delta\theta} \leq t \leq t_k + \Delta t \frac{r}{\Delta\theta} \tag{26}$$

where t_k is the epoch at which the kernel scan circle has been acquired. The same holds for the samples entering in each patch.

5.2 Matching Two Surveys, the Crossing Problem

The patching algorithm asses independency between patches and avoids pile up, but does not gives a fast way to assess for each patch in the first survey what is the corresponding patch in the second survey.

The patching algorithm is used to define the list of kernel circles and patches in the first survey. The subsequent algorithm is used to define the list of kernel circles in the second survey. The principle of the algorithm is illustrated in Fig. 6. Here P_1 and P_2 are at the crossing point of Kernel 1 and Kernel 2, while P_3 and P_4 of Kernel 1 and Kernel 3, with $t_1 < t_2 < t_3$, Kernel 1 belonging to the first survey while Kernel 2 and Kernel 3 to the second.

The mathematical details of crossing are reported in the next section, while testing cases in App. A.

5.2.1 Crossing Formulation

Given a pixel $\mathbf{P}$ of coordinates λ, δ (longitude and latitude) compute the scan circles crossing the pixel and the crossing condition with the following hypothesis

1. scan circles have an angular radius $0° < \beta \leq 90°$;
2. scan circles axis lies on the spherical equator;

5.2.2 The Solution

The circle crossing the pixel $\mathbf{P}$ is defined by its angular radius β and the coordinates of its center λ_{cc}, δ_{cc}. The second of the hypothesys asssures that $\delta_{cc} \equiv 0$ and that condition for crossing is

$$|\delta| \leq \beta. \tag{27}$$

The problem reduces to the determination of λ_{cc} and of the phase φ_{cc} on the circle.

The centers of the crossing circles are determined noting that they lie on a circle centered on $\mathbf{P}$ and with radius β. Taking a carthesian coordinates system defined by the meridian circle passing per $\mathbf{P}$ (equivalent to assume $\lambda = 0$) the equation for the points on the circle of centers $\check{\mathbf{C}}$ is

$$\check{\mathbf{C}}(\varphi, \delta, \beta) = \begin{pmatrix} \cos\beta\cos\delta \\ 0 \\ \cos\beta\sin\delta \end{pmatrix} + \begin{pmatrix} \cos\delta & 0 & -\sin\delta \\ 0 & 1 & 0 \\ \sin\delta & 0 & \cos\delta \end{pmatrix} \begin{pmatrix} 0 \\ \sin\beta\sin\varphi \\ \sin\beta\cos\varphi \end{pmatrix}, \tag{28}$$

where $\varphi = 0$ when z has the most positive value (crossing the $\mathbf{P}$ meridian with the most positive latitude).

The longitude λ_{cc} is given by the points crossing the equator i.e. solving the equation

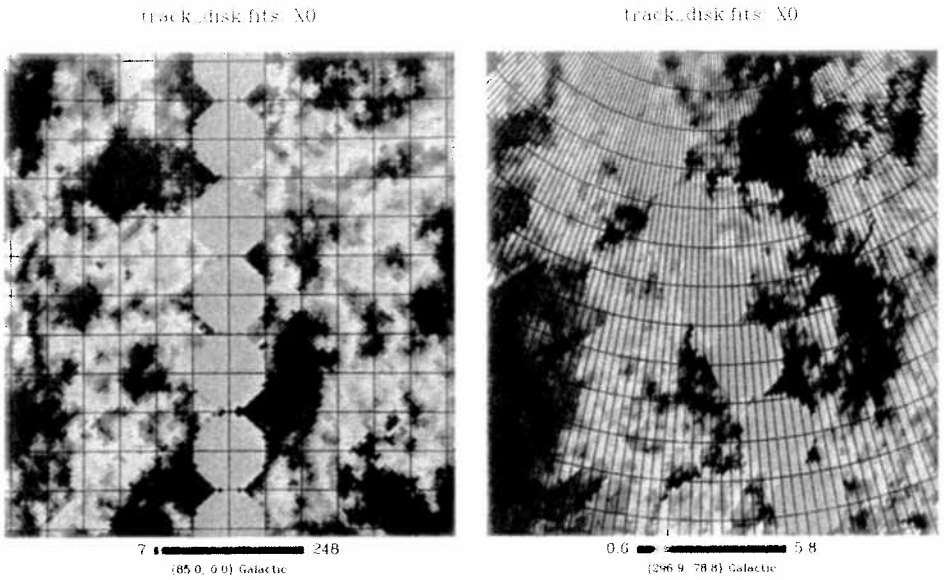

Figure 5: Details from Fig. 4, frames are centered on circles with phase angles of 0° (left) and 50° (right).

$$\cos\beta\sin\delta + \cos\delta\sin\beta\cos\varphi_{cc} = 0, \tag{29}$$

with solutions [6]

$$\varphi_{cc,\pm} = \pm\arccos\frac{\cos\beta\sin\delta}{\sin\beta\cos\delta}. \tag{30}$$

From solution (30) values of λ_{cc} are readily extracted from

$$\begin{aligned}\cos\lambda_{cc} &= \cos\beta\cos\delta - \sin\delta\sin\beta\cos\varphi_{cc}\\ \sin\lambda_{cc} &= \sin\beta\sin\varphi_{cc}\end{aligned} \tag{31}$$

but since $\beta \leq 90°$ then $\lambda_{cc} \leq 90°$

$$\lambda_{cc,\pm} = \arcsin(\sin\beta\sin\varphi_{cc}), \tag{32}$$

while the most general case $\lambda \neq 0$ has solution

$$\lambda_{cc,\pm} = \lambda + \arcsin(\sin\beta\sin\varphi_{cc}). \tag{33}$$

The phases of the intersections are recovered from the equation of the scan circle $\check{\mathbf{S}}$ with equation

$$\check{\mathbf{S}}(\varphi,\lambda_{cc},\beta) = \begin{pmatrix}\cos\beta\cos\lambda_{cc}\\ \cos\beta\sin\lambda_{cc}\\ 0\end{pmatrix} + \begin{pmatrix}\cos\lambda_{cc} & -\sin\lambda_{cc} & 0\\ \sin\lambda_{cc} & \cos\lambda_{cc} & 0\\ 0 & 0 & 1\end{pmatrix}\begin{pmatrix}0\\ \sin\beta\sin\varphi\\ \sin\beta\cos\varphi\end{pmatrix}, \tag{34}$$

the pixel is crossed for $\varphi = \varphi_{pxl}$ solution of the equation

[6] Note that the solutions exists if $|\cos\beta\sin\delta| \geq |\sin\beta\cos\delta|$, equivalent to condition (27).

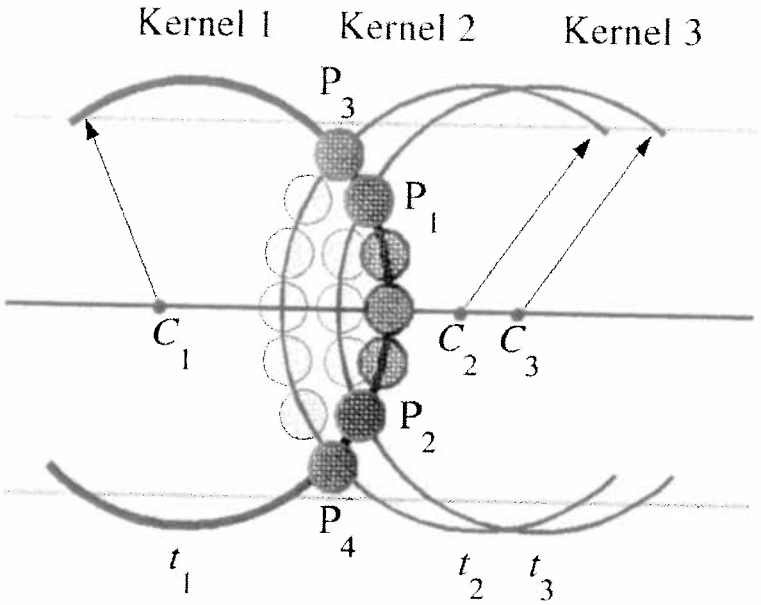

Figure 6: Crossing algorithm and patching for the second scan survey.

$$\check{\mathbf{S}}(\varphi_{\mathrm{pxl}}, \lambda_{\mathrm{cc}}, \beta) = \begin{pmatrix} \cos\delta \\ 0 \\ \sin\delta \end{pmatrix}, \tag{35}$$

so that

$$\varphi_{\mathrm{pxl},\pm} = \pm \arccos\left(\frac{\sin\delta}{\sin\beta}\right). \tag{36}$$

5.2.3 The Algorithm

From λ, δ, β there are at most two solutions defined as 1 and 2 so that there are the following subcases

case $|\delta| > \beta$,

No solution exists.

case $|\delta| == 0$,

$$\varphi_{\mathrm{cc},1} = \frac{1}{2}\pi, \quad \lambda_{\mathrm{cc},1} = \lambda - \beta, \quad \varphi_{\mathrm{pxl},1} = \frac{3}{2}\pi; \tag{37}$$

$$\varphi_{\mathrm{cc},2} = \frac{3}{2}\pi, \quad \lambda_{\mathrm{cc},2} = \lambda + \beta, \quad \varphi_{\mathrm{pxl},2} = \frac{1}{2}\pi; \tag{38}$$

case $|\delta| == \beta$,

$$\varphi_{\mathrm{cc},1} = \pi, \quad \lambda_{\mathrm{cc},1} = \lambda, \quad \varphi_{\mathrm{pxl},1} = 0; \tag{39}$$

$$\varphi_{\mathrm{cc},2} = \pi, \quad \lambda_{\mathrm{cc},2} = \lambda, \quad \varphi_{\mathrm{pxl},2} = 0; \tag{40}$$

case $0 < \delta < \beta$,

$$\varphi_{\mathrm{cc},1} = \varphi_{\mathrm{cc}}, \quad \lambda_{\mathrm{cc},1} = \lambda - \lambda_{\mathrm{cc}}, \quad \varphi_{\mathrm{pxl},1} = 2\pi - \varphi_{\mathrm{pxl}}; \tag{41}$$

$$\varphi_{\mathrm{cc},2} = 2\pi - \varphi_{\mathrm{cc}}, \quad \lambda_{\mathrm{cc},2} = \lambda + \lambda_{\mathrm{cc}}, \quad \varphi_{\mathrm{pxl},2} = \varphi_{\mathrm{pxl}}; \tag{42}$$

case $-\beta < \delta < 0$, Da completare questo caso

$$\varphi_{\rm cc,1} = \varphi_{\rm cc}, \quad \lambda_{\rm cc,1} = \lambda - \lambda_{\rm cc}, \quad \varphi_{\rm pxl,1} = 2\pi - \varphi_{\rm pxl}; \tag{43}$$

$$\varphi_{\rm cc,2} = 2\pi - \varphi_{\rm cc}, \quad \lambda_{\rm cc,2} = \lambda + \lambda_{\rm cc}, \quad \varphi_{\rm pxl,2} = \varphi_{\rm pxl}; \tag{44}$$

with the ancillary quantities $\varphi_{\rm cc}$, $\lambda_{\rm cc}$, $\varphi_{\rm pxl}$ defined as

$$\varphi_{\rm cc} = \arccos \frac{\cos\beta \sin\delta}{\sin\beta \cos\delta}; \tag{45}$$

$$\lambda_{\rm cc} = \arcsin(\sin\beta \sin\varphi_{\rm cc}); \tag{46}$$

$$\varphi_{\rm pxl} = \arccos\left(\frac{\sin\delta}{\sin\beta}\right). \tag{47}$$

6 Transforms between the ecliptic and the map reference frame

Equations to transform pointing directions, spacecraft positions and sun positions between the ecliptic and the map reference frame are given in this section.

The map reference frame is a swapped corotating reference frame based on the cloud reference frame.

The cloud reference frame is a reference frame where the cloud exhibits cylindrical symmetry. So its origin coincides with the cloud center, its equatorial plane with the symmetry plane of the cloud. Its $\hat{Z}$ axis is the symmetry axis of the cloud. Here we assume that the cloud reference frame has $\hat{X}$ axis corresponding to the ascending node of the cloud symmetry plane as seen in the ecliptic reference frame, and $\hat{Y}$ normal to $\hat{X}$ and $\hat{Z}$ and oriented to form a right-handed reference frame.

The corotating reference frame has $\hat{Z}$ axis defined by the $\hat{Z}$ axis of the cloud reference frame, $\hat{Y}$ axis defined by the cloud-center to spacecraft direction [7] and $\hat{X}$ axis orthogonal to the two in order to define a right-handed reference frame.

The map reference frame is the corotating reference frame but with $\hat{Y}$ and $\hat{Z}$ swapped in order to take advantage of the organisation of the ring ordered `HEALPix` pixelization scheme.

From ecliptical refer frame to Cloud Refer Frame $\mathcal{R}_{\rm ME} = \mathcal{R}_{{\rm ME},i}\mathcal{R}_{{\rm ME},\Omega}$

$$\mathcal{R}_{{\rm ME},i} = \begin{pmatrix} 1 & 0 & 0 \\ 0 & \cos i & \sin i \\ 0 & -\sin i & \cos i \end{pmatrix}, \quad \mathcal{R}_{{\rm ME},\Omega} = \begin{pmatrix} \cos\Omega & \sin\Omega & 0 \\ -\sin\Omega & \cos\Omega & 0 \\ 0 & 0 & 1 \end{pmatrix}. \tag{48}$$

From Cloud r.f. to Corotating r.f.

$$\mathcal{R}_{{\rm CM},\omega} = \begin{pmatrix} \cos\omega & \sin\omega & 0 \\ -\sin\omega & \cos\omega & 0 \\ 0 & 0 & 1 \end{pmatrix}. \tag{49}$$

From corotating reference frame to the Map reference frame

$$\mathcal{R}_{\rm MCM} = \begin{pmatrix} 0 & -1 & 0 \\ 0 & 0 & 1 \\ 1 & 0 & 0 \end{pmatrix}. \tag{50}$$

The algorithm to determine the transform from ecliptic coordinates to the map, corotating coordinates starting from the PLANCK position $\mathbf{R}_{\rm P}$ is the following:

[7] An alternative definition would be to take the $\hat{Y}$ axis defined by the cloud-center to L_2 direction.

1.. Converts the $\mathbf{R}_{\rm P}$ position to the center of the cloud in the ecliptic reference frame

$$\mathbf{R}'_p = \mathbf{R}_{\rm P} - \mathbf{R}_{0,c}. \tag{51}$$

2.. Rotates the position vector to cloud refer frame

$$\mathbf{R}'_{p,C} = \mathcal{R}_{\rm ME}\mathbf{R}'_p \tag{52}$$

3.. Determines latitude and longitude trigonometric functions ($\mathbf{e}'_x$, $\mathbf{e}'_y$, $\mathbf{e}'_z$ are the unitary vectors for the corotating reference frame)

$$\begin{aligned}
\widehat{\mathbf{R}}'_{p,C} &= \mathbf{R}'_{p,C} / \left|\mathbf{R}'_{p,C}\right| \\
\sin\theta &= \widehat{\mathbf{R}}'_{p,C} \cdot \mathbf{e}'_z \\
\cos\theta &= \sqrt{1-\sin^2\theta} \\
\sin\omega &= \widehat{\mathbf{R}}'_{p,C} \cdot \mathbf{e}'_y / \cos\theta \\
\cos\omega &= \widehat{\mathbf{R}}'_{p,C} \cdot \mathbf{e}'_x / \cos\theta
\end{aligned} \tag{53}$$

If $\cos\theta = 0$ then it is assumed $\sin\omega = 0$, $\cos\omega = 1$.

4.. Determines the components of $\mathbf{R}'_{p,C}$ in the intermediate corotating reference frame:

$$\begin{aligned}
R'_{p,x} &= R'_{p,C,x}\cos\omega + R'_{p,C,y}\sin\omega \\
R'_{p,y} &= -R'_{p,C,x}\sin\omega + R'_{p,C,y}\cos\omega \\
R'_{p,z} &= R'_{p,C,z}
\end{aligned} \tag{54}$$

Note that the computation of the y component in this case may be skipped, since it is 0 by definition.

5.. Swaps the axis to obtain the map reference frame

$$R^{\rm M}_{p,x} = -R'_{p,0}, \quad R^{\rm M}_{p,y} = R'_{p,z}, \quad R^{\rm M}_{p,z} = R'_{p,y}. \tag{55}$$

6.. For the Sun position $\mathbf{R}_\odot$

$$\mathbf{R}'_\odot = \mathcal{R}_{\rm ME}(\mathbf{R}_\odot - \mathbf{R}_{0,c}), \tag{56}$$

$$\mathbf{R}'_\odot = \begin{cases} R'_{\odot,x} = R'_{\odot,C,x}\cos\omega + R'_{\odot,C,y}\sin\omega \\ R'_{\odot,y} = -R'_{\odot,C,x}\sin\omega + R'_{\odot,C,y}\cos\omega \\ R'_{\odot,z} = R'_{\odot,C,z} \end{cases} \tag{57}$$

$$R^{\rm M}_{\odot,x} = -R'_{\odot,0}, \quad R^{\rm M}_{\odot,y} = R'_{\odot,z}, \quad R^{\rm M}_{\odot,z} = R'_{\odot,y}. \tag{58}$$

7.. For pointing

$$\mathbf{P}' = \mathcal{R}_{\rm ME}\mathbf{P}, \tag{59}$$

$$\mathbf{P}'_C = \begin{cases} P'_x = P'_{C,x}\cos\omega + P'_{C,y}\sin\omega \\ P'_y = -P'_{C,x}\sin\omega + P'_{C,y}\cos\omega \\ P'_z = P'_{C,z} \end{cases} \tag{60}$$

$$P^{\rm M}_x = -P'_0, \quad P^{\rm M}_y = P'_z, \quad P^{\rm M}_z = P'_y. \tag{61}$$

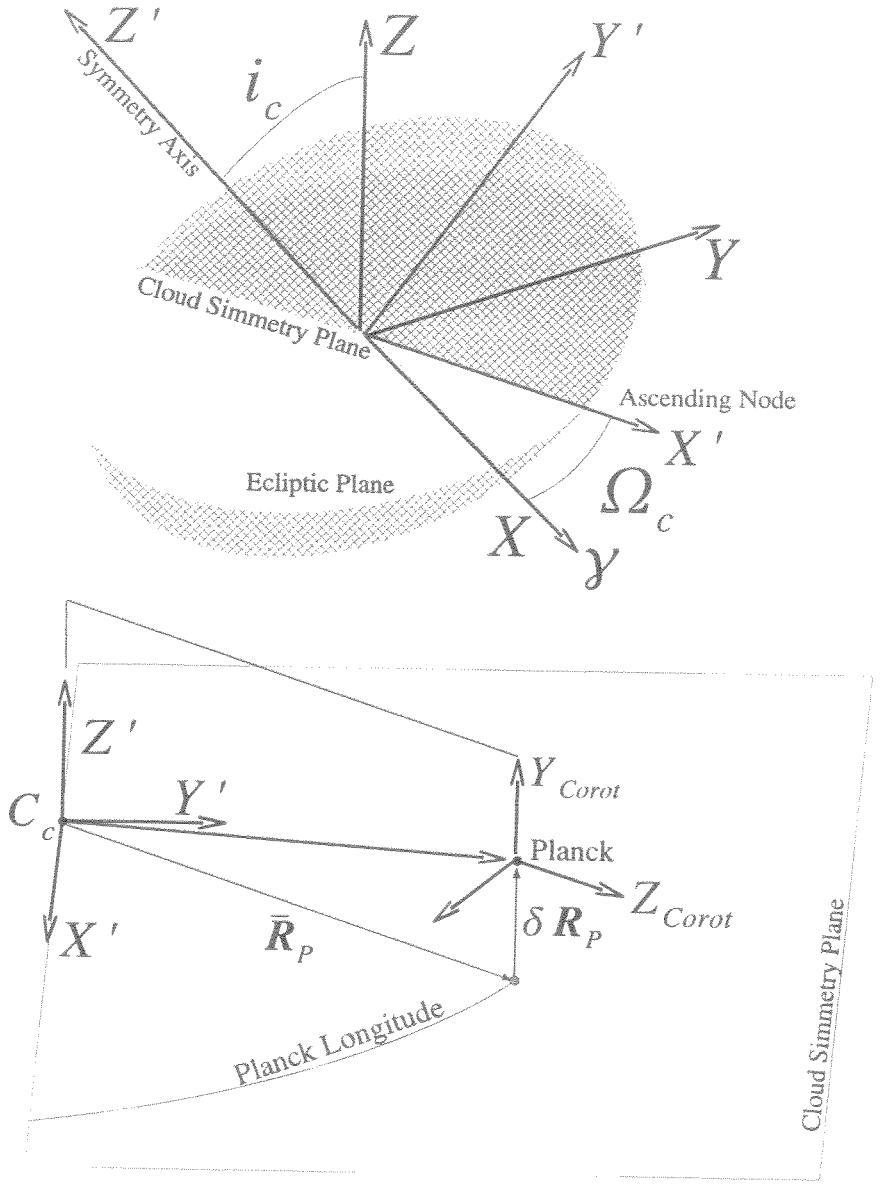

Figure 7: Relations between the cloud-centred ecliptic reference frame, the cloud symmetry reference frame and the spacecraft centred corotating reference frame. Top panel angles between the cloud-centred Ecliptical reference frame (full yellow disc - black arrows), and the cloud cylindrical symmetry reference frame (dashed blue disc - red arrows). Bottom panel angles between the cloud cylindrical symmetry reference frame, the cloud-centred corotating cylindrical reference frame, the spacecraft - centred corotating reference frame. The (in this case above the symmetry plane) displacement of PLANCK, $\delta\mathbf{R}_P$, respect to the constant reference position, $\bar{\mathbf{R}}_P$, assumed to be in the symmetry plane of the corotating reference frame is also displayed. The graph are not in scale with real distances.

7 Conclusion

In this report we outlined some technical details relevant for simulations that have not been included in Maris et al. (2005) for sake of conciseness. We focused here on the numerical code, its validation, the detailed series expansion of the ZLE, the algorithm for creation of the circular sky patches, the definition of colour and emissivity correction, the transforms between the relevant reference systems, and some details on file formats.

Acknowledgements – We warmly acknowledge the PLANCK collaboration teams for having provided us with instrument and mission details. We thank F. Boulanger and M. Juvela, W.T. Reach for constructive discussions and J.P. Bernard, G. Cremonese, M. Fulle, and G. De Zotti for encouraging and stimulating conversations. Some of the results in this report have been derived using the `HEALPix` package (Górsky et al. 2005). M.M. acknowledges also L. Abrami and C. Doz for help in recovering bibliographic material.

References

Challinor, A.D., Anthony, D., Mortlock, D.J., van Leeuwen, F., Lasenby, A.N., et al., 2002, MNRAS, 331, 994

Dupac, X., & Tauber, J., 2005, A&A, 430, 363

Fixsen, D.J., & Dwek, E., 2002, Ap.J., 578, 1009

Górski, K.M., Hivon, E., Banday, A.J., Wandelt, B.D., Hansen, F.K., et al., 2005, ApJ, 622, 759

Kelsall, T., Weiland, J.T., Franz, B.A., Reach, W.T., Arendt, R.G., et al., 1998, ApJ, 508, 44 (also astro-ph/9806250)

Maris, M., 2001, PLANCK/*LFI - FS_ZOD: A Simulator of the Zodiacal Light Emission for the* PLANCK *Mission*, 2001, Planck/LFI Int.Rep.: PL-LFI-OAT-TN-023, Issue 1.0

Maris, M., Fogliani, S., Burigana, C., 2004, *How to use the Zodiacal Light Emission Maps for* PLANCK , Planck/LFI Int.Rep.: PL-LFI-OAT-TN-031, Issue 1.0, 2004, Dec 31th

Maris, M., Burigana, C., Fogliani, S., 2005, *Zodiacal Light Emission in the* PLANCK *mission*, A&A, submitted, June 28, 2005

Pasian, F., & Sygnet, J.-F., 2002, Proc. of *Astronomical Data Analysis II*, Edts. Starck, J.-L., Murtagh, F. D. Proceedings of the SPIE, 4847, 25

Reach, W.T., Abergel, A., Boulanger, F., Desert, F.-X., Perault, M., et al., 1996, A&A, 315, L381

Reach, W.T., Morris, P., Boulanger, F., Okumura, K., 2003, Icarus, 164, 384

van Leeuwen, F., Challinor, A.D., Mortlock, D.J., Ashdown, M.A.J., Hobson, M.P., et al., 2002, MNRAS, 331, 975

Wheelock, S.L., Gautier, T.N., Chillemi, J., Kester, D., McCallon, H., et al., 1994, IRAS Sky Survey Atlas Explanatory Supplement, JPL Pubbl. 94-11

A Validation of Crossing Algorithm

The following examples are usefull to validate the crossing algorithm. The results and the constructions have been validated with the aid of an armillary sphere.

A.1 Circle full-radius above the equator

$$\lambda = 0°, \quad \delta = 45.0°, \quad \beta = 45°$$

$$\lambda_{cc} = 0°, \quad \varphi_{cc} = 0°, \quad \varphi_{pxl} = 0°$$

$$\varphi_{cc,1} = 0°, \quad \lambda_{cc,1} = 0°, \quad \varphi_{pxl,1} = 360°$$

$$\varphi_{cc,2} = 360°, \quad \lambda_{cc,2} = 0°, \quad \varphi_{pxl,2} = 0°$$

A.2 Circle half-radius above the equator

$$\lambda = 0°, \quad \delta = 22.5°, \quad \beta = 45°$$

$$\lambda_{cc} = 40.0604°, \quad \varphi_{cc} = 65.5302°, \quad \varphi_{pxl} = 57.2349°$$

$$\varphi_{cc,1} = 65.5302°, \quad \lambda_{cc,1} = -40.0604°, \quad \varphi_{pxl,1} = 302.7651°$$

$$\varphi_{cc,2} = 294.4698°, \quad \lambda_{cc,2} = +40.0604°, \quad \varphi_{pxl,2} = 57.2349°$$

A.3 Circle on the equator

$$\lambda = 0°, \quad \delta = 0°, \quad \beta = 45°$$

$$\lambda_{cc} = 45°, \quad \varphi_{cc} = 90°, \quad \varphi_{pxl} = 90°$$

$$\varphi_{cc,1} = 90°, \quad \lambda_{cc,1} = -45°, \quad \varphi_{pxl,1} = 270°$$

$$\varphi_{cc,2} = 270°, \quad \lambda_{cc,2} = 45°, \quad \varphi_{pxl,2} = 90°$$

A.4 Circle half-radius below the equator

$$\lambda = 0°, \quad \delta = -22.5°, \quad \beta = 45°$$

$$\lambda_{cc} = 40.0604°, \quad \varphi_{cc} = 114.4698°, \quad \varphi_{pxl} = 122.7651°$$

$$\varphi_{cc,1} = 114.4698°, \quad \lambda_{cc,1} = -40.0604°, \quad \varphi_{pxl,1} = 237.2349°$$

$$\varphi_{cc,2} = 245.53020°, \quad \lambda_{cc,2} = +40.0604°, \quad \varphi_{pxl,2} = 122.7651°$$

A.5 Circle full-radius below the equator

$$\lambda = 0°, \qquad \delta = -45.0°, \quad \beta = 45°$$

$$\lambda_{cc} = 0°, \qquad \varphi_{cc} = 180°, \quad \varphi_{pxl} = 180°$$

$$\varphi_{cc,1} = 180°, \quad \lambda_{cc,1} = 0°, \quad \varphi_{pxl,1} = 180°$$

$$\varphi_{cc,2} = 180°, \quad \lambda_{cc,2} = 0°, \quad \varphi_{pxl,2} = 180°$$

A.6 Circle above the equator, tested with the sphere

Note that in this case the accuracy is about 0.5°.

Numerical Calculation

$$\lambda = 0°, \qquad \delta = 20.6122°, \qquad \beta = 41.9319°$$

$$\lambda_{cc} = 37.3617°, \qquad \varphi_{cc} = 65.2461°, \qquad \varphi_{pxl} = 58.2096°$$

$$\varphi_{cc,1} = 65.2461°, \quad \lambda_{cc,1} = -37.3617°, \quad \varphi_{pxl,1} = 301.7904°$$

$$\varphi_{cc,2} = 294.7539°, \quad \lambda_{cc,2} = +37.3617°, \quad \varphi_{pxl,2} = 58.2096°$$

Measured on the Sphere

$$\lambda = 0°, \qquad \delta = 20.6122°, \qquad \beta = 41.9319°$$

$$\lambda_{cc} = 37.5717°, \quad \varphi_{cc} = ---°, \qquad \varphi_{pxl} = 58.7902°$$

$$\varphi_{cc,1} = ---°, \quad \lambda_{cc,1} = -37.5717°, \quad \varphi_{pxl,1} = 301.2098°$$

$$\varphi_{cc,2} = ---°, \quad \lambda_{cc,2} = +37.5717°, \quad \varphi_{pxl,2} = 58.7902°$$

A.7 Circle below the equator, tested with the sphere

Note that in this case the accuracy is about 0.5°.

Numerical Calculation

$$\lambda = 0°, \qquad \delta = -20.6122°, \qquad \beta = 41.9319°$$

$$\lambda_{cc} = 37.3617°, \qquad \varphi_{cc} = 65.2461°, \qquad \varphi_{pxl} = 121.7904°$$

$$\varphi_{cc,1} = 114.7539°, \quad \lambda_{cc,1} = -37.3617°, \quad \varphi_{pxl,1} = 238.2097°$$

$$\varphi_{cc,2} = 245.2471°, \quad \lambda_{cc,2} = +37.3617°, \quad \varphi_{pxl,2} = 121.7904°$$

Measured on the Sphere

$\lambda = 0°$, $\delta = -20.6122°$, $\beta = 41.9319°$

$\lambda_{\mathrm{cc}} = 37.5717°$, $\varphi_{\mathrm{cc}} = ---°$, $\varphi_{\mathrm{pxl}} = 58.7902°$

$\varphi_{\mathrm{cc},1} = ---°$, $\lambda_{\mathrm{cc},1} = -37.5717°$, $\varphi_{\mathrm{pxl},1} = 238.2097°$

$\varphi_{\mathrm{cc},2} = ---°$, $\lambda_{\mathrm{cc},2} = +37.5717°$, $\varphi_{\mathrm{pxl},2} = 121.7900°$